The EMBO Journal (2006) 25, 4020–4032 | © 2006 European Molecular Biology Organization | All Rights Reserved 0261-4189/06
www.embojournal.org

THE EMBO JOURNAL

Mitogen-activated protein kinases interacting kinases are autoinhibited by a reprogrammed activation segment

Ralf Jauch[1,2,*], Min-Kyu Cho[3], Stefan Jäkel[4], Catharina Netter[5], Kay Schreiter[4], Babette Aicher[4], Markus Zweckstetter[3], Herbert Jäckle[1] and Markus C Wahl[5,*]

[1]Max-Planck-Institut für Biophysikalische Chemie, Abteilung Molekulare Entwicklungsbiologie, Göttingen, Germany, [2]Genome Institute of Singapore, Laboratory for Structural Biochemistry, Singapore, [3]Max-Planck-Institut für Biophysikalische Chemie, NMR-basierte Strukturbiologie, Göttingen, Germany, [4]DeveloGen AG, Göttingen, Germany and [5]Max-Planck-Institut für Biophysikalische Chemie, Abteilung Zelluläre Biochemie/Röntgenkristallographie, Göttingen, Germany

Autoinhibition is a recurring mode of protein kinase regulation and can be based on diverse molecular mechanisms. Here, we show by crystal structure analysis, nuclear magnetic resonance (NMR)-based nucleotide affinity studies and rational mutagenesis that nonphosphorylated mitogen-activated protein (MAP) kinases interacting kinase (Mnk) 1 is autoinhibited by conversion of the activation segment into an autoinhibitory module. In a Mnk1 crystal structure, the activation segment is repositioned via a Mnk-specific sequence insertion at the N-terminal lobe with the following consequences: (i) the peptide substrate binding site is deconstructed, (ii) the interlobal cleft is narrowed, (iii) an essential Lys–Glu pair is disrupted and (iv) the magnesium-binding loop is locked into an ATP-competitive conformation. Consistently, deletion of the Mnk-specific insertion or removal of a conserved phenylalanine side chain, which induces a blockade of the ATP pocket, increase the ATP affinity of Mnk1. Structural rearrangements required for the activation of Mnks are apparent from the cocrystal structure of a Mnk2^{D228G}–staurosporine complex and can be modeled on the basis of crystal packing interactions. Our data suggest a novel regulatory mechanism specific for the Mnk subfamily.

The EMBO Journal (2006) **25,** 4020–4032. doi:10.1038/sj.emboj.7601285; Published online 17 August 2006
Subject Categories: proteins; structural biology
Keywords: autoinhibition; drug design; mitogen-activated protein kinases interacting kinase; Mnk1 and Mnk2; protein kinase regulation

*Corresponding authors. R Jauch, Genome Institute of Singapore, 60 Biopolis Street, #02-01, Genome, Singapore 138672. Tel.: +65 6478 8653; E-mail: jauchr@gis.a-star.edu.sg or MC Wahl, Max-Planck-Institut für Biophysikalische Chemie, Abteilung Zelluläre Biochemie/Röntgenkristallographie, Am Faßberg 11, 37077 Göttingen, Germany. Tel.: +49 551 201 1046; Fax: +49 551 201 1197; E-mail: mwahl@gwdg.de

Received: 20 March 2006; accepted: 25 July 2006; published online: 17 August 2006

Introduction

Mitogen-activated protein (MAP) kinases interacting kinases (Mnks) phosphorylate the eukaryotic translation initiation factor 4E (eIF4E) (Waskiewicz *et al*, 1997, 1999; Scheper *et al*, 2001) and factors that bind to AU-rich elements in the 3′-untranslated region of certain mRNAs (Buxade *et al*, 2005). Via these activities, Mnks apparently regulate the expression of a specific set of proteins (Nikolcheva *et al*, 2002; Walsh and Mohr, 2004; Buxade *et al*, 2005) rather than global protein synthesis (O'Loghlen *et al*, 2004b; Ueda *et al*, 2004; Reiling *et al*, 2005). Mnks are involved in growth control (Reiling *et al*, 2005), inflammation (Nikolcheva *et al*, 2002; Buxade *et al*, 2005) and viral translation (Walsh and Mohr, 2004) and, therefore, represent interesting targets for pharmaceutical intervention.

Mnks comprise a subfamily of Ser/Thr kinases (Manning *et al*, 2002). Phylogenetically they are placed into the group of Ca^{2+}/calmodulin-dependent kinases (CaMK) (Manning *et al*, 2002), although, like many other CaMK group members, they are not regulated by Ca^{2+}/calmodulin (Slentz-Kesler *et al*, 2000). Mnks are activated through phosphorylation by the growth factor-stimulated Ras/extracellular signal-regulated kinase pathway and the stress-induced p38 pathway (Fukunaga and Hunter, 1997; Waskiewicz *et al*, 1997). There are two human Mnk genes, *mnk1* and *mnk2*, each of which gives rise to alternatively spliced isoforms (Mnk1a, Mnk1b, Mnk2a and Mnk2b) spanning 347–465 residues (Scheper *et al*, 2003; O'Loghlen *et al*, 2004a). All four proteins bear a stretch of basic residues at their N-termini that functions as a nuclear localization signal and as a binding region for the eukaryotic initiation factor 4G. Mnk1a and Mnk2a contain putative nuclear export motifs and MAP kinase-binding sites C-terminal of the central kinase domains, both of which are removed by alternative splicing in Mnk1b and Mnk2b. Here, we investigated the catalytic domains of Mnk1 and Mnk2, which are ~80% sequence identical and are not affected by alternative splicing.

The catalytic domains of protein kinases (PKs) encompass conserved structural elements for binding of ATP and the peptide substrates and for phosphoryl transfer. Therefore, the structures of active-state PKs closely resemble each other, whereas the structures of inactive-state kinases are diverse (Huse and Kuriyan, 2002; Nolen *et al*, 2004). Tight control of PK activities is essential for intracellular signaling cascades. Switching between inactive and active PK conformations can be achieved by diverse mechanisms, such as phosphorylation/dephosphorylation (Canagarajah *et al*, 1997; Krupa *et al*, 2004), release/binding of autoinhibiting domains (Goldberg *et al*, 1996; Kobe *et al*, 1996; Mol *et al*, 2004a) and interaction with regulatory subunits (Jeffrey *et al*, 1995) or by a combination of these strategies (Russo *et al*, 1996). Consequently, there is no generic molecular mechanism for inactivating PKs. Yet, it is crucial for the development of

specific inhibitors to understand the regulation of individual kinases in detail.

We have recently reported the crystal structure of the nonphosphorylated Mnk2 catalytic domain (Jauch *et al*, 2005), in which the enzyme exhibited a noncanonical extended arrangement of the activation segment and an ATP-competitive conformation of the magnesium-binding Asp-Phe-Asp (DFD) motif. The latter motif is conserved as an Asp-Phe-Gly (DFG) sequence in other kinases. The significance of the extended activation segment and the reason why the protein prefers the inhibitory DFD motif conformation remained elusive. Here, we present the crystal structures of the Mnk1 catalytic domain and of a Mnk2 active site mutant in complex with staurosporine, which provide an explanation for this architecture. Our results reveal that in nonphosphorylated Mnk1 the activation segment is converted into an autoinhibitory module. Autoinhibition encompasses impaired ATP binding and peptide substrate positioning, primarily mediated by a Mnk-specific sequence insertion within the activation segment. Solution nuclear magnetic resonance (NMR) studies on wild-type (wt) and mutant enzymes together with homology modeling and structural comparisons support this mode of autoinhibition in Mnk1 and suggest that Mnk2 is autoinhibited by a similar mechanism. The ensemble of Mnk structures now available highlight structural transitions accompanying Mnk activation.

Results

Overall architecture of the Mnk1 catalytic domain

We produced a polypeptide spanning residues 37–341 of Mnk1 in *Escherichia coli* and purified it to homogeneity. It includes the catalytic domain of Mnk1 and is henceforth referred to as Mnk1-kinase region (Mnk1-KR). Similarly to Mnk2-KR (Jauch *et al*, 2005), this fragment recapitulates the activity of the full-length protein in that it phosphorylates an eIF4E peptide only after activation by ERK2 *in vitro* (data not shown). Mnk1-KR could be crystallized and the structure could be solved and refined to 2.8 Å resolution, including anisotropic data to 2.5 Å resolution (Table I). The asymmetric unit contains two Mnk1-KR molecules related by a noncrystallographic two-fold axis. Although one molecule exhibits lower temperature factors and a clearer electron density in several regions, the functionally important regions are virtually identical in both molecules. The final model encompasses residues 39–335 of Mnk1.

Mnk1-KR displays the bilobal makeup of PKs (Knighton *et al*, 1991). The N-terminal lobe contains a twisted sheet of five antiparallel β-strands (β1–β5) and the regulatory helix αC (Figures 1 and 2A). It harbors the elements essential for ATP binding such as the glycine-rich loop (GR-loop), a conserved Lys78 in strand β3 and a conserved Glu94 in helix αC. The predominantly α-helical C-terminal lobe contains the elements required for peptide substrate binding and phosphate transfer, including the catalytic loop (C-loop, residues 170–175 in Mnk1), the magnesium-binding loop, and the activation segment (residues 194–235; Figures 1 and 2A). The magnesium-binding loop of Mnks contains a noncanonical DFD motif (residues 191–193 in Mnk1) instead of the otherwise highly conserved DFG motif (Hanks *et al*, 1988; Taylor and Radzio-Andzelm, 1994; Hanks, 2003). Two sections of the Mnk1-KR exhibit extensive conformational flexibility and could not be traced in the electron density. First, the core of the activation segment including the activation loop and the P + 1 loop (residues 197–222) and second, a region encompassing helix αG (residues 261–290), which has been shown to comprise a Zn^{2+}-coordinating motif in Mnk2 (Jauch *et al*, 2005), possibly involved in substrate binding (Dar *et al*, 2005). In the present structure, the Zn^{2+}-binding site may be disordered owing to a lack of crystal packing interactions that stabilized the motif in Mnk2-KR crystals. Although we could not detect Zn^{2+} in the Mnk1-KR crystals by X-ray fluorescence (not shown), the high conservation of four cysteines in the latter region suggests that the Zn^{2+}-binding site is a general feature of Mnks. Zn^{2+} binding may be stabilized by interacting factors *in vivo*.

The activation segment is repositioned at the N-terminal lobe

In active PKs, the P + 1 loop and the following helix αEF are buried within the kinase core in an environment provided by

Table I Diffraction data collection and refinement statistics

Structure	*Mnk1-KR*	*Mnk2-KR^{D228G}–staurosporine*
Data collection		
Space group	$P4_32_12$	$P3_221$
Cell dimensions		
a, *b*, *c* (Å)	93.5, 93.5, 175.2	102.4, 102.4, 76.4
α, β, γ (deg)	90, 90, 90	90, 90, 120
Resolution (Å)	30.0–2.8 (2.9–2.8)	30.0–2.7 (2.8–2.7)
R_{sym}[a]	10.7 (35.5)	9.0 (58.1)
$I/\sigma(I)$	13.1 (2.3)	17.0 (3.0)
Completeness (%)	92.1 (50.0)	99.7 (99.6)
Redundancy	8.2 (4.9)	5.8 (5.0)
Refinement		
Resolution (Å)	30.0–2.8 (2.5)[b]	30.0–2.7
Reflections (No./%)	18206/89.8	12218/99.7
R_{work}/R_{free}[c]	20.7/25.7	20.1/24.6
No. of atoms		
Protein	3815	2165
Water oxygens	138	21
Sulfate ions	2	—
Staurosporine	—	1
B-factors		
Chain A	39.3	69.5
Chain B	57.7	—
Water	41.0	72.4
Sulfate ions	63.1	—
Staurosporine	—	52.0
Ramachandran analysis (%)		
Preferred	98.8	98.0
Generally allowed	1.0	0.8
Disallowed	0.2	1.2
R.m.s. deviations from ideal		
Bond lengths (Å)	0.010	0.010
Bond angles (deg)	1.1	1.4

[a]$R_{sym}(I) = (\sum_{hkl}\sum_i[|I_i(hkl) - \langle I(hkl)\rangle|]/\sum_{hkl}\sum_i[I_i(hkl)]$; $I_i(hkl)$—intensity of the *i*th measurement of *hkl*; $\langle I(hkl)\rangle$—average value of *hkl* for all *i* measurements.
[b]Data up to 2.5 Å resolution have been included in the refinement. Statistics for data between 2.8 and 2.5 Å resolution: R_{sym}—34.9 %; $I/\sigma(I)$—2.1; completeness—25.8 %; redundancy—4.1.
[c]$R_{work} = \sum_{hkl}[||F_{obs}| - k|F_{calc}||]/\sum_{hkl}[|F_{obs}|]$;
$R_{free} = \sum_{hkl\subset T}[||F_{obs}| - k|F_{calc}||]/\sum_{hkl\subset T}[|F_{obs}|]$; $hkl \subset T$—test set.

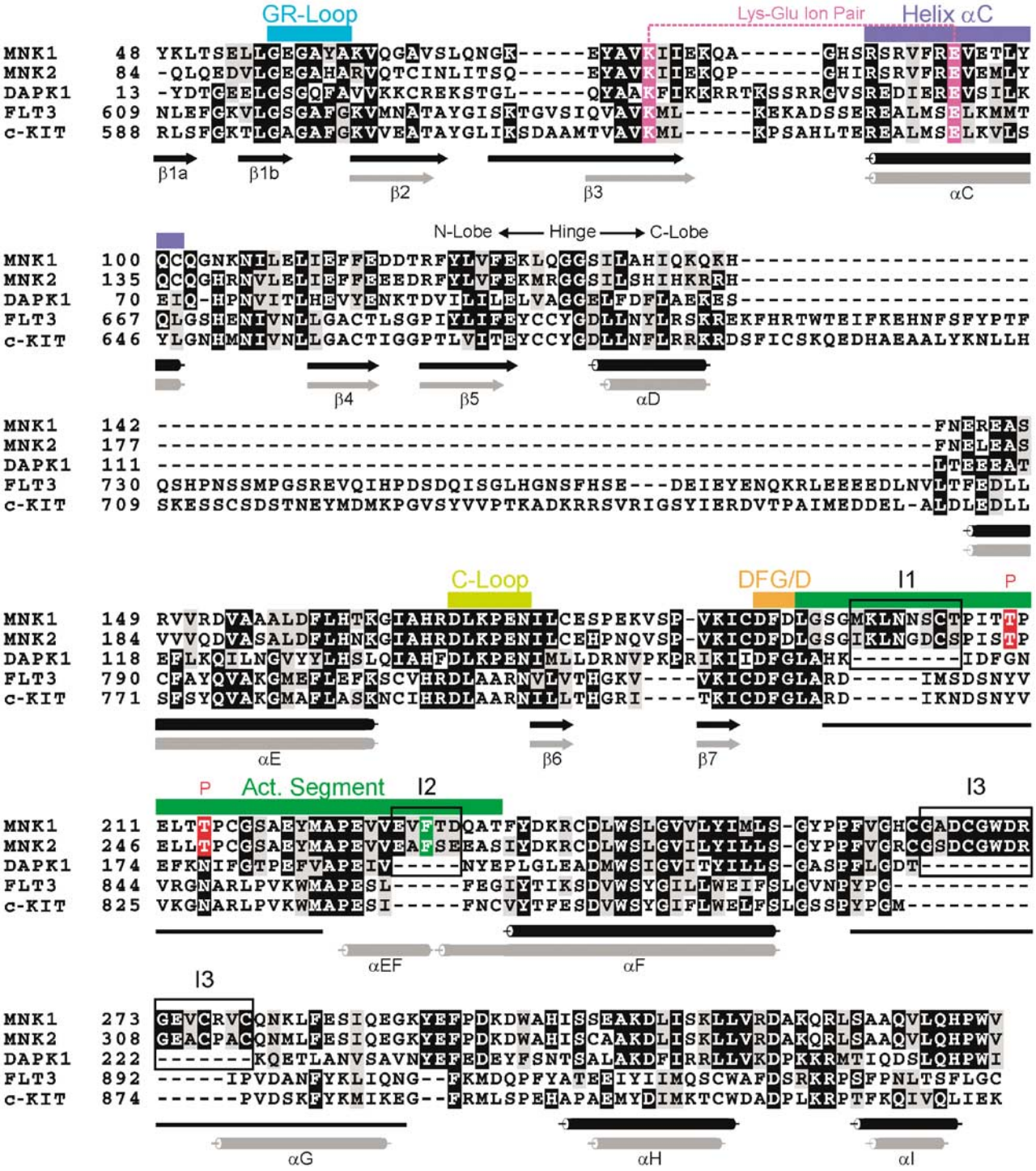

Figure 1 Sequence comparison. Multiple sequence alignment of Mnk1, Mnk2, DAPK1, Flt3 (SwissProt ID P36888) and c-KIT (NCBI entry code NP000222) spanning the kinase domains. The DAPK1-Mn^{2+}-AMPPNP cocrystal structure (Tereshko *et al*, 2001) represents a CaMK group member in the active state. c-KIT (Mol *et al*, 2004b) and Flt3 (Griffith *et al*, 2004) are receptor tyrosine kinases, in which autoinhibition via an N-terminal JM domain (not shown) resembles autoinhibition via the activation segment in Mnk1 (see Discussion). The alignment was made with T-Coffee (Notredame *et al*, 2000), shaded with BoxShade (http://www.ch.embnet.org/software/BOX_form.html) and edited manually. A darker background indicates a higher conservation. Functional elements are color-coded and labeled: tip of the glycine-rich loop (GR-loop)—cyan; Lys–Glu ion pair—magenta; helix αC—blue; catalytic loop (C-loop)—yellow; DFG/D motif—orange; activation segment—green. This coloring scheme is maintained in the following structure figures. The background of the conserved Lys–Glu pair is shown in magenta, the background of the Mnk-specific Phe230/Phe265 (Mnk1/Mnk2) of the activation segment in green. Insertions that are specific for Mnks within the CaMK group (I1–I3) are boxed. The hinge region separates the N- and C-terminal lobes as indicated. Phosphorylation sites are shown in red (labeled 'P'). Secondary structure elements as found in Mnk1-KR (this work) and Mnk2-KR (Jauch *et al*, 2005) (PDB-ID 2AC3) are given below the alignment (Mnk1—black, Mnk2—gray). Note that in this and the following figures, we refer to the Mnk-specific activation segment, which is expanded and includes αEF and the αEF/αF loop (see the text for details).

the C-loop and helices αF and αG (Knighton *et al*, 1991). In this position, the P + 1 loop can interact with the peptide substrate at the residue following the phosphorylation site. The short helix αEF is connected to helix αF through the αEF/αF loop, which varies in size and sequence among different PKs (Nolen *et al*, 2004). In Mnk1-KR, helix αEF, designated by the highly conserved Ala-Pro-Glu (APE) motif, is unwound. The region corresponding to αEF and the αEF/αF loop is detached from the C-terminal lobe and traverses the interlobal cleft (Figures 2A and 3A). The APE motif and residues from the αEF/αF loop line up with helix αC at the N-terminal lobe (Figures 2A and 3A). As a consequence, the N-terminal lobe is displaced towards the C-terminal lobe and thereby narrows the interlobal cleft (Figure 2A and B). Furthermore, repositioning of the αEF-αEF/αF loop region demands that the P + 1 loop be concomitantly disengaged from the C-terminal lobe, impairing the peptide substrate-binding site. Hence, the current positioning of the P + 1 loop and the helix αEF-αEF/αF loop region is incompatible with kinase activity.

The activation segment of Mnk1 is reorganized

The 'activation segment' of a PK traditionally refers to the section delineated by the DFG and APE motifs. At its core, the 'activation loop' designates the region typically undergoing structural reorganization upon activation/inactivation (Nolen *et al*, 2004). In Mnk1-KR, however, the region subjected to structural reorganization extends to αEF and the αEF/αF loop (Figures 1, 2A and 3A). Thus, the Mnk-specific activation segment is expanded and includes, in contrast to previous conventions (Nolen *et al*, 2004), αEF and the αEF/αF loop. The structure of Mnk1-KR therefore represents the most extensive rearrangement of an activation segment reported to date.

The inhibitory conformation of the activation segment in Mnk1-KR likely reflects structural consequences of an amino-acid insertion (I2; Figure 1) within the αEF/αF loop. I2 is conserved in Mnks but is absent from other CaMK group PKs (Figure 1). Residues of insertion I2 are instrumental in stabilizing the autoinhibitory conformation seen in Mnk1-KR (e.g. Glu228 and Phe230; see below). Thus, in nonphosphorylated Mnk1-KR, insertion I2 constitutes a key determinant leading to the reprogramming of the activation segment into an autoinhibitory module. Another Mnk-specific insertion (I1) is located C-terminal of the DFD motif and is disordered in the present structure.

Phosphate-binding residues stabilize the autoinhibited structure

The inactive conformation of nonphosphorylated Mnk1-KR is stabilized by ionic interactions involving conserved Arg residues. First, Arg90 and Arg93 from helix αC contact Glu225 (APE motif) and Glu228 (αEF/αF loop), respectively, thereby fastening the activation segment to the N-terminal lobe (Figure 3C). Second, Arg169 upstream of the catalytic loop (the RD-Arg) forms an ion pair with Asp238 (not shown). The RD-Arg and the Arg residues from helix αC are known to form the so-called RD-pocket, which in activated PKs accommodates phosphorylated residues from the activation segment (Krupa *et al*, 2004; Nolen *et al*, 2004). The interaction between such phosphorylated residues and the RD-pocket correctly positions the activation segment for substrate binding at the C-terminal lobe (Nolen *et al*, 2004). Thus, the phosphate groups introduced during activation will provide alternative interaction sites for the RD-pocket residues, most likely leading to a disruption of the intramolecular interactions seen in Mnk1-KR and thereby releasing the activation segment from the N-terminal lobe.

The repositioned activation segment locks an ATP-competitive conformation

The first Asp of the DFG motif at the beginning of the activation segment is invariant among catalytically active PKs and is known to coordinate a magnesium ion that is essential for phosphoryl transfer (Adams, 2001). The region encompassing the DFG motif has therefore been termed the magnesium-binding loop. Mnks contain a DFD motif at the corresponding positions. In active kinases, the Phe of the DFG/D motif is situated in a pocket, which in Mnk1-KR is provided by Thr97 and Leu98 (emanating from helix αC), His168 (upstream of the C-loop), Ile107, Leu161 and Ile189. This active DFG/D motif conformation is referred to as DFG/D-in and its corresponding binding site will henceforth be referred to as DFG/D-in pocket.

The conformation of the activation segment in the present Mnk1-KR structure has a pronounced effect on the DFD motif. Phe230, which emanates from the Mnk-specific αEF/αF loop insertion I2 and is conserved in the Mnk subfamily (Figure 1), comes to lie in the DFG/D-in pocket (Figures 3A and C). It thereby displaces the DFD motif, which in turn is rotated by $\sim 180^\circ$ around the Φ angle of Asp191 ($\Phi_{Asp191} = -110^\circ$) with respect to the DFG/D-in conformation of active-state PKs ($\Phi_{Asp191,\ DAPK1} = 55^\circ$) (Tereshko *et al*, 2001). Phe192 of the DFD motif, in turn, occupies a hydrophobic pocket provided by Val63, Leu108, Phe124 (the 'gatekeeper residue') and Leu177, which would normally accommodate the adenosyl moiety of ATP. The resulting DFD conformation is referred to as DFG/D-out and is incompatible with ATP binding.

The Mnk-specific DFD stabilizes the DFG/D-out conformation

The DFG/D-out conformation in Mnk1-KR is stabilized by a network of unconventional interactions. Both, the invariant Asp191 and the Mnk-specific Asp193 of the DFD motif are engaged in tight carboxyl–carboxyl side chain interactions with the active site residues Glu94 and Asp170, respectively (Figure 4A). The two contacting oxygens of the carboxylate groups are 2.5–2.6 Å apart in both instances, which is significantly shorter than the average O–O distance in nonacidic hydrogen bonds (Flocco and Mowbray, 1995). These arrangements suggest that the interacting carboxylates are partially protonated. As described for other such carboxyl–carboxyl interactions (Werten *et al*, 2002), the Asp191–Glu94 and Asp193–Asp170 pairs are stabilized by neighboring amines (Lys78) or amides (Asn175), respectively (Figure 4A). Attractive carboxyl–carboxyl side chain interactions are often observed in protein structures and are particularly abundant within the catalytic centers of enzymes (Flocco and Mowbray, 1995).

Glu94 and Asp170 correspond to residues that are invariant among catalytically active PKs (Hanks *et al*, 1988). Glu94 originates from the regulatory helix αC and is known to form an ion pair with Lys78 that is essential for productive ATP binding (Adams, 2001). This pairing is obstructed in Mnk1-KR, because Asp191 of the DFD motif is wedged

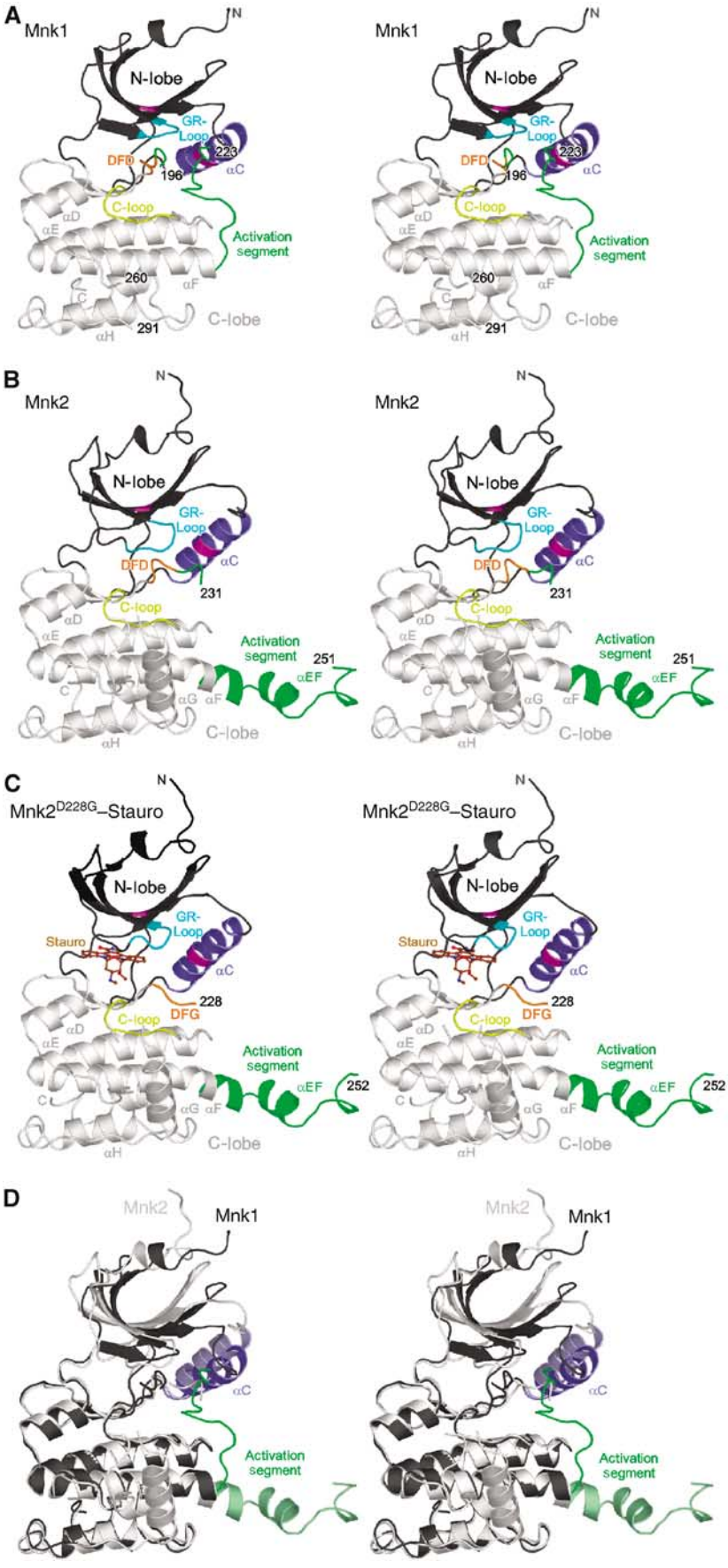

between Glu94 and Lys78 (Figure 4A). Asp170 corresponds to the catalytic Asp residue of the C-loop (Figure 4A).

Comparison of Mnk1-KR and Mnk2-KR crystal structures

Recently, we have reported the crystal structure of Mnk2-KR (Jauch *et al*, 2005). Mnk1 and Mnk2 exhibit 78% sequence identity within their catalytic domains, both enzymes are activated by similar cellular stimuli and their reported substrate specificities are identical (Waskiewicz *et al*, 1999; Scheper *et al*, 2001). It is therefore surprising that the crystal structures of Mnk1-KR and Mnk2-KR exhibit pronounced differences in the relative orientations of the lobes, in the conformations of the activation segments and in atomic details of the DFG/D-out conformations (Figures 2A, B and

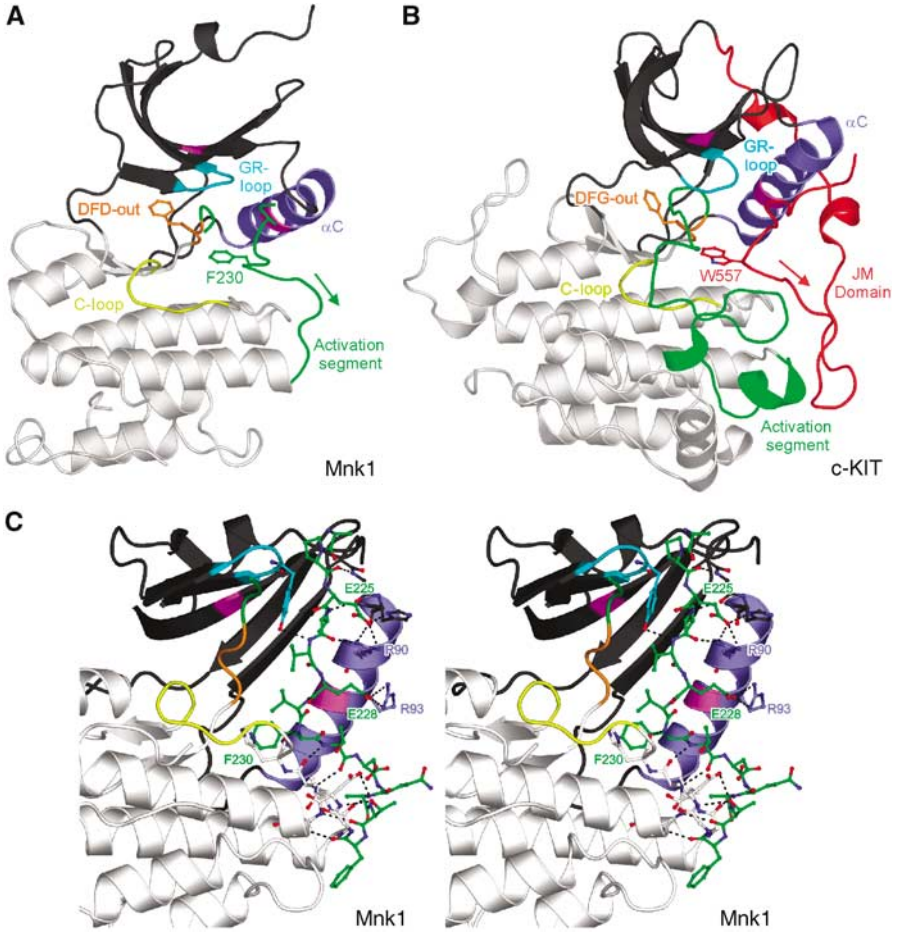

Figure 3 Autoinhibitory conformation of the activation segment. (**A**) Ribbon plot of Mnk1-KR. A region corresponding to helix αEF and the αEF/αF loop traverses the interlobal cleft from the N- to the C-terminal lobe (direction: green arrow). Phe230 (ball-and-stick) of the Mnk-specific insertion I2 in the activation segment occupies the DFG/D-in pocket, thereby pushing Phe192 (ball-and-stick) of the DFD motif into the ATP-binding pocket. (**B**) Ribbon plot of c-KIT (Mol *et al*, 2004b) (PDB ID 1T45). The autoinhibitory JM domain is shown in red. It crosses the interlobal cleft from the N- to the C-terminal lobe (red arrow). Trp557 (ball-and-stick) of the JM domain is mechanistically analogous to Phe230 in Mnk1-KR. The activation segment of c-KIT is fully visible in contrast to Mnk1-KR. (**C**) Close-up stereo ribbon plot showing the activation segment of Mnk1-KR folding back across the interlobal cleft and lining up with helix αC. The activation segment and interacting residues are shown in ball-and-stick. Hydrogen bonds and salt bridges that tether the activation segment are shown as dashed lines. Two Arg residues of helix αC and two interacting Glu residues of the activation segment are labeled. The molecule has been rotated 45° about the horizontal axis (top to back) compared to Figure 1A.

Figure 2 Overall folds of Mnk kinases. Stereo ribbon plots of the Mnk kinases. The N-terminal lobes are shown in dark gray, the C-terminal lobes in light gray. All structural figures were prepared with PyMol (http://pymol.sourceforge.net/). (**A**) Overall structure of Mnk1-KR. If not mentioned otherwise, the same orientation of the kinase and the same relative orientations of other kinases are maintained in all following figures. The coloring scheme for functional elements is the same as in Figure 1 and is maintained in the following figures: tip of the glycine-rich loop (GR-loop)—cyan; Lys–Glu ion pair—magenta; helix αC—blue; catalytic loop (C-loop)—yellow; DFG/D motif—orange; activation segment—green. The activation loop and the P + 1 loop (residues 197–222) and a Mnk-specific cysteine cluster and helix αG (residues 261–290) could not be modeled (terminal residues indicated). (**B**) Overall structure of Mnk2-KR (determined in Jauch *et al*, 2005) after alignment of its C-terminal lobe on Mnk1-KR. Compared to Mnk1-KR, the N-terminal lobe of Mnk2-KR adopts an open conformation with respect to the C-terminal lobe. The N-terminal portion of the activation segment (residues 232–250, Mnk2 numbering) could not be modeled (terminal residues indicated). (**C**) Overall structure of the Mnk2-KR^{D228G}–staurosporine complex after alignment of its C-terminal lobe on Mnk1-KR. No pronounced global conformational changes are observed upon staurosporine binding compared to the apo-Mnk2-KR (B). The N-terminal portion of the activation segment (residues 229–251, Mnk2 numbering) could not be modeled (terminal residues indicated). (**D**) Stereo ribbon plot comparing Mnk1-KR (dark gray with helix αC in blue and the activation segment in green) with Mnk2-KR (lighter colors) after superimposition via the C-terminal lobes, depicting the different relative orientations of the two lobes.

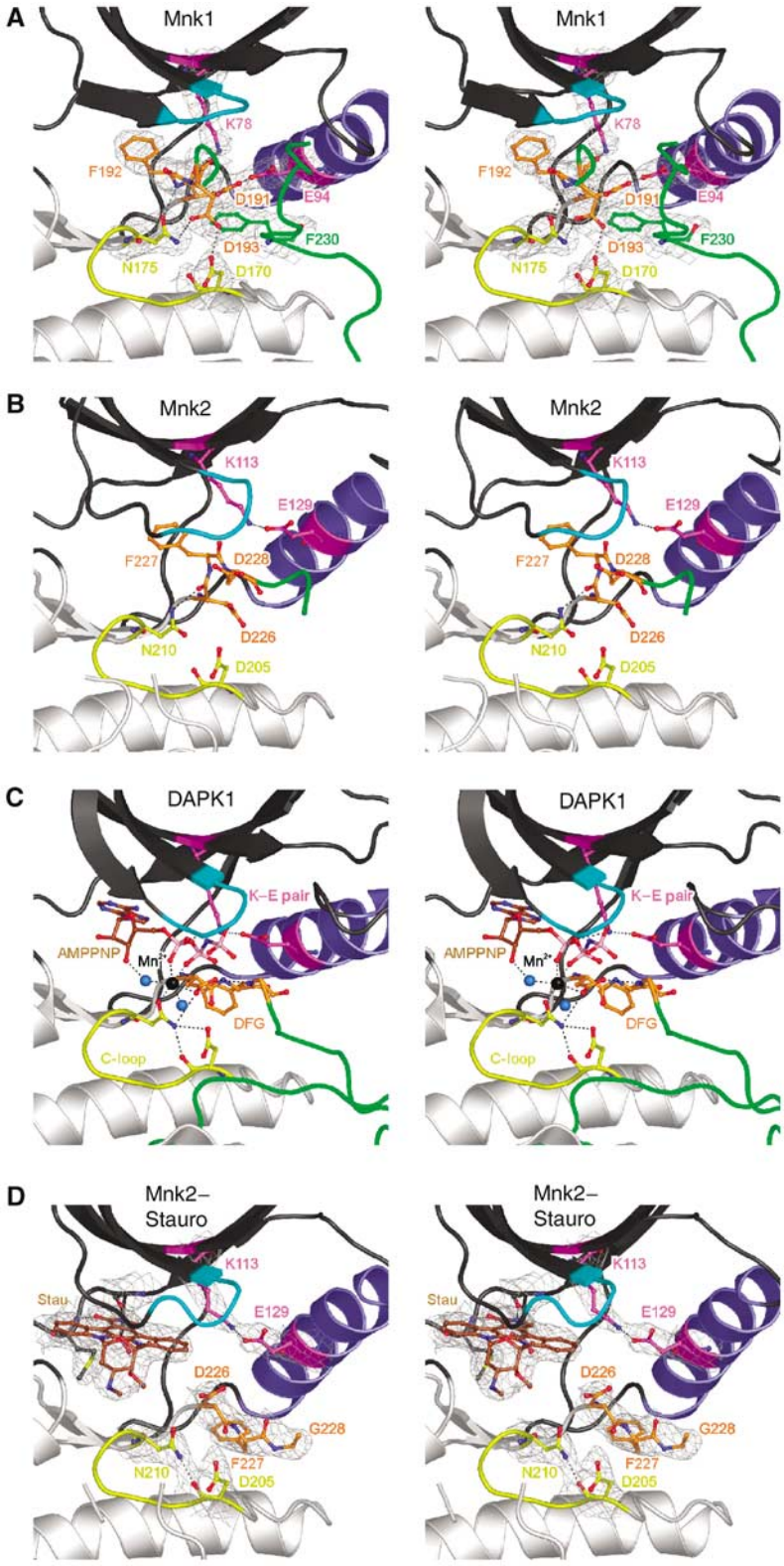

Figure 4 ATP binding and DFG/D pockets. Stereo diagrams depicting details of the ATP and DFG/D pockets. Critical residues are labeled. Hydrogen bonds and ionic interactions are depicted by dashed lines. (**A**) Mnk1-KR with an ionic interaction network involving the Asp residues of the DFD motif. The conserved Lys–Glu ion pair is broken. The final $2F_o-F_c$ electron density (gray; contoured at the 1σ level) is shown covering selected residues. (**B**) Mnk2-KR (Jauch *et al*, 2005) (PDB-ID 2AC3) in which the DFD-out conformation is retained, although the activation segment has been detached from the N-terminal lobe. No clear interaction involving the Asp residues of the DFD motif can be discerned. (**C**) DAPK1-Mn^{2+}–AMPPNP complex (Tereshko *et al*, 2001) (PDB ID 1IG1). The AMPPNP is shown in ball-and-stick (carbon—brown; phosphorus—pink; Mn^{2+}—black sphere; water—blue spheres). (**D**) Mnk2–KR^{D228G}–staurosporine complex. Staurosporine is shown in ball-and-stick (carbon—brown). Note the complete reversal of the DFD-out to the DFD-in conformation upon staurosporine binding (compare to panel B). The final $2F_o$–F_c electron density (gray; contoured at the 1σ level) is shown covering staurosporine and selected residues.

4A, B). In the Mnk2-KR structure, the activation segment protrudes from the kinase core and helix αF is prolonged by one turn. Furthermore, Mnk2-KR displays an ordered P + 1 loop and a helical conformation in αEF, whereas these QJ;elements are disordered (P + 1) or structurally rearranged (helix αEF and αEF/αF loop) in Mnk1-KR. The N-terminal lobe of Mnk2-KR is tilted by approximately 10° compared to Mnk1-KR, leading to an opening of the ATP binding mouth (Figures 2A and B) and explaining the absence of acid–acid interactions involving the DFD motif in the Mnk2-KR structure.

The conformation of Mnk2-KR in the crystal is stabilized by extensive packing interactions involving the protruding activation segment. In solution, Mnk2-KR may adopt a structure resembling Mnk1-KR. In order to investigate whether Mnk1 and Mnk2 adopt similarly autoinhibited conformations in solution, we determined relative nucleotide affinities of wt and mutant enzymes.

Mutational analysis supports the mechanism of autoinhibition in Mnks

ATP binding to nonphosphorylated Mnk1-KR appears to be inhibited on two levels: (i) the Mnk-specific activation segment 'locks' the DFG/D-out conformation because Phe230 occupies the DFG/D-in pocket and (ii) the Mnk-specific Asp of the DFD motif stabilizes the DFG/D-out conformation by acid–acid interactions. We reasoned that this dual-level control should be reflected in significantly higher nucleotide affinities of the phosphorylated kinases compared to the nonphosphorylated forms and intermediate affinities in nonphosphorylated mutants lacking Phe230 or the Mnk-specific DFD-Asp. We had previously tested ATP binding to phosphorylated and nonphosphorylated Mnk2-KR using a dot-blot assay but were not able to determine relative affinities (Jauch *et al*, 2005). We therefore employed the saturation transfer difference (STD) NMR method to monitor magnetization transfer from protein to bound AMPPNP, a nonhydrolyzable ATP analog. STD-NMR is a versatile and robust screening method that selectively detects protein-bound nucleotides for a wide range of affinities (McCoy *et al*, 2005). Although it is difficult to determine absolute K_d's by STD-NMR, the method can reliably detect relative affinities even for low-affinity interactions as in the present case.

Nonphosphorylated Mnk1-KR only showed a very weak STD signal, indicating that it bound only minute amounts of AMPPNP (Figure 5). Interaction with the nucleotide was significantly enhanced upon phosphorylation (Figure 5). As expected, nonphosphorylated Mnk1-KR mutants, in which insertion I2 (residues 228–232) had been deleted or in which Phe230 was converted into an alanine, bound AMPPNP at intermediate degrees (Figure 5). In each case, bound AMPPNP could be released by the addition of staurosporine. Staurosporine is a nonspecific kinase inhibitor with nanomolar to low micromolar K_d's for most Ser/Thr kinases that competes with ATP at its canonical binding site (Tamaoki *et al*, 1986; Lawrie *et al*, 1997; Prade *et al*, 1997). Thus, all AMPPNP binding detected occurred at the canonical ATP pockets of the enzymes. These results support the role of Phe230 and of the Mnk-specific insertion I2 in stabilizing the ATP-competitive DFD-out conformation.

Nonphosphorylated Mnk2-KR exhibited higher residual AMPPNP affinity than Mnk1-KR but once again nucleotide binding was significantly enhanced upon phosphorylation (Figure 5). Again as expected, the affinity of AMPPNP to the nonphosphorylated Mnk2-KR^{D228G} mutant, in which the DFD motif had been converted to a DFG motif, was intermediate between that of nonphosphorylated and phosphorylated wt Mnk2-KR (Figure 5). Again staurosporine competed with AMPPNP binding in each case (Figure 5A). These findings are consistent with the Mnk-specific Asp of the DFD motif (Asp228 in Mnk2) stabilizing the inhibitory DFG/D-out conformation in Mnk2, in agreement with its enrollment in acid–acid interactions as seen in Mnk1-KR. The observation that conversion of the DFD to a DFG motif does not fully restore the nucleotide affinity of the phosphorylated wt enzyme is consistent with the idea that the ATP-competitive conformation of Mnk2-KR in solution is reinforced by a Mnk1-KR-like repositioning of the activation segment.

Different stringency of autoinhibition in Mnk1 and Mnk2

Nonphosphorylated Mnk2-KR exhibited higher residual affinity to AMPPNP than nonphosphorylated Mnk1-KR (Figure 5A, right panel). This observation suggests that the activation segment in nonphosphorylated Mnk2-KR exhibits conformational fluctuations that allow ATP to partially 'squeeze' into its binding site and reverse the inhibitory DFD-out conformation, whereas nonphosphorylated Mnk1-KR is more stringently controlled and adopts an ATP-receptive conformation to a lesser extent. In order to explain these differences, we used the Mnk1-KR structure as a scaffold and converted all residues to the Mnk2 sequence. In the resulting Mnk2-KR homology model, most intramolecular contacts involving the repositioned activation segment were maintained by identical or highly homologous residues with two exceptions: (i) in Mnk1-KR, the Tyr60 hydroxyl group hydrogen bonds to the backbone carbonyl of Asp193 (DFD motif) and to the backbone amide of Val227 (neighboring insertion I2) and thereby stabilizes the autoinhibitory conformation (not shown). Mnk2 contains His95 at the respective position, whose side chain may be less suited to engage in similar interactions. (ii) The side chain of Thr97 of Mnk1-KR hydrogen bonds to the backbone carbonyls of Arg93 and Phe230. It is replaced by Met132 in Mnk2, which cannot support similar interactions and may weaken the alignment of the αEF-αEF/αF loop region with helix αC. Taken together, our data support the notion that Mnk1 and Mnk2 are regulated by a fundamentally similar mechanism but that because of a few amino-acid replacements autoinhibition is tighter in Mnk1 than in Mnk2. Our observation of a tighter autoinhibition in Mnk1 agrees with the previous notion that Mnk2 exhibits a higher basal activity compared to Mnk1 (Parra *et al*, 2005).

Staurosporine induces a DFG/D-in conformation after unlocking

We next sought direct evidence for the hypothesis that the Mnk2-KR crystal structure was unlocked with respect to the inhibitory DFG/D-out conformation and that ATP binding additionally demands a switch from the DFG/D-out to the DFG/D-in conformation. To this end, we performed cocrystallization and soaking experiments with ATP, AMPPNP or staurosporine. Derivatizing Mnk1-KR or Mnk2-KR crystals with any of the compounds by either technique failed. For Mnk2-KR^{D228G}, however, we were able to determine a

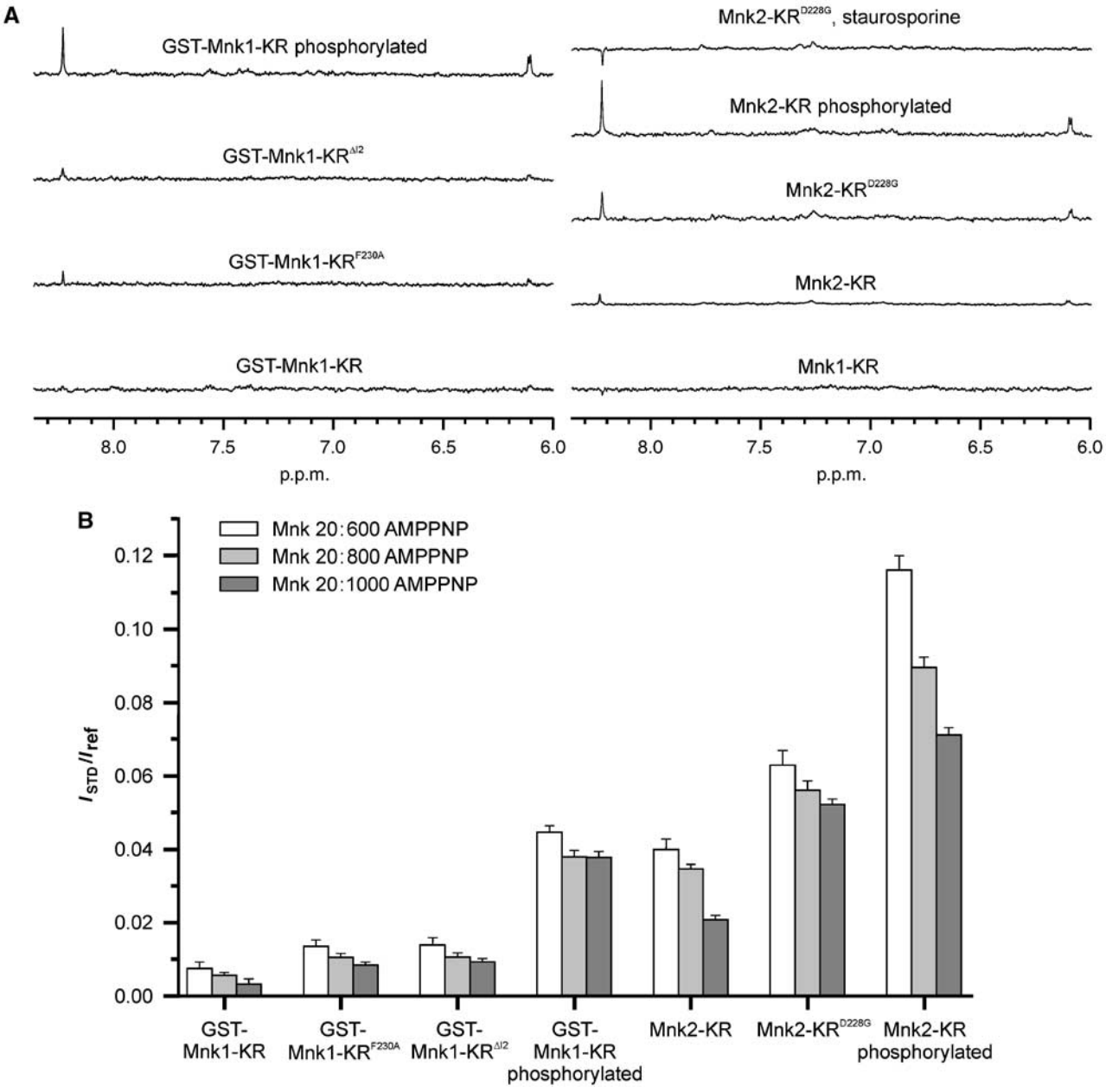

Figure 5 AMPPNP binding. (**A**) STD-NMR spectra of 0.6 mM AMPPNP (1.0 mM AMPPNP for Mnk1-KR, lower right) binding to 20 μm enzyme covering the region of the strong NMR signals of H2 (8.22 p.p.m.) and H6 (6.10 p.p.m.) of AMPPNP. Left panel: spectra of Mnk1-KRs all retaining the N-terminal GST tag. Right panel: spectra of Mnk1-KR and Mnk2-KRs without the tag. The top-right spectrum was recorded after addition of 0.1 mM staurosporine to an NMR sample containing 2.0 mM AMPPNP and 20 μM Mnk2-KR^{D228G}. The negative peaks seen in this spectrum were also seen in the spectrum of AMPPNP alone. Identical NMR parameters were used for each spectrum acquisition. (**B**) Fractional STD effects (I_{STD}/I_{ref}) of AMPPNP (H2 proton) in the presence of nonphosphorylated GST-Mnk1-KR, nonphosphorylated GST-Mnk1-KR^{F230A}, nonphosphorylated GST-Mnk1-KR$^{\Delta I2}$, phosphorylated GST-Mnk1-KR, nonphosphorylated Mnk2-KR, nonphosphorylated Mnk2-KR^{D228G} or phosphorylated Mnk2-KR. The protein concentration was kept fixed (20 μM) and the AMPPNP concentration was increased: 0.6 mM—white; 0.8 mM—light gray; 1.0 mM—gray. The fractional STD effect (I_{STD}/I_{ref}) decreases with increasing excess of AMPPNP. Note that the trends in the relative affinities are independent of the AMPPNP concentration. Maximum errors based on the signal-to-noise ratio are indicated.

staurosporine cocrystal structure at 2.7 Å resolution (Table I). As expected, staurosporine binds at the canonical ATP pocket in a fashion similar to its known binding mode in other PKs (Lawrie *et al*, 1997; Prade *et al*, 1997) (Figures 2C and 4D). The polycyclic ring system of the drug is sandwiched between the β-sheet of the N-terminal lobe and the short two-stranded β6–β7 sheet of the C-terminal lobe (Figure 4D). The N1 and O5 atoms of staurosporine engage in hydrogen bonds to the backbone carbonyl of Glu160 and the backbone nitrogen of Met162 of the hinge region, respectively (Figure 4D). Similar hydrogen bonds are fostered by the adenine base of ATP when bound to PKs (Prade *et al*, 1997). Significantly, binding of staurosporine elicited a complete switch of the DFG motif from the DFG/D-out to the DFG/D-in conformation (Figure 4D). The resulting conformation of Mnk2-KR^{D228G} provides a nucleotide-binding pocket, which could likewise accept an ATP molecule. This observation indicates that binding of ATP requires a similar switch of the DFD motif,

which in turn would require a previous removal of the Phe residue of the activation segment from the DFG/D-in pocket. Furthermore, these results suggest that binding of an ATP-competitive substance and thus presumably of ATP at the nucleotide-binding site is sufficient to induce the DFG/D-in conformation after unlocking.

Discussion

Our results show that nonphosphorylated members of the Mnk subfamily are autoinhibited by reprogramming of the activation segment into an autoinhibitory module. Residues in a Mnk-specific insertion (I2, located within the αEF/αF loop) and in the unwound helix αEF interact with helix αC of the N-terminal lobe and thereby disable canonical peptide substrate positioning. Furthermore, the repositioned activation segment places a Phe from insertion I2 into the DFG/D-in pocket, which locks the DFD motif in an ATP-competitive DFG/D-out conformation.

Activation of Mnks involves phosphorylation at two sites within the activation loop (Waskiewicz *et al*, 1999; Scheper *et al*, 2001; Ueda *et al*, 2004). Phosphorylation most likely provides alternative interaction sites for Arg residues that stabilize the autoinhibited state. The residues to become phosphorylated reside at the core of the activation segment, which is disordered in the present Mnk1-KR structure and thus presumably is accessible to the activating kinases. Therefore, the repositioned activation segment not only silences the enzymes but also presents phosphorylation target residues to the activating kinases.

Interestingly, the receptor tyrosine kinases c-KIT (Mol *et al*, 2004b) and Flt3 (Griffith *et al*, 2004) also achieve autoinhibition by plunging a hydrophobic residue into the DFG/D-in pocket and thereby reinforcing a DFG/D-out conformation (Figure 3B). However, the blocking residue in c-KIT and Flt3 originates from a specialized autoinhibiton module, the juxtamembrane (JM) domain that connects a transmembrane helix to the catalytic domain on the cytoplasmic side (Griffith *et al*, 2004; Mol *et al*, 2004b). This JM domain lies outside the kinase core as opposed to the situation in Mnks, in which the blocking residue (Phe230/Phe265 in Mnk1/Mnk2) originates from the activation segment.

Differences in the AMPPNP affinities of the nonphosphorylated Mnks suggest that the degree of autoinhibition may be fine-tuned in the different isoforms. Intriguingly, the lower residual AMPPNP affinity in nonphosphorylated Mnk1-KR compared to nonphosphorylated Mnk2-KR correlates with a lower basal activity of the Mnk1 isoform in cell culture assays (Parra *et al*, 2005). It may be explained by a small number of amino-acid substitutions as suggested by our homology model. However, based on the overall trends of the differential nucleotide-binding analysis we expect that Mnk1 and Mnk2 are regulated by a fundamentally similar mechanism.

Our crystal structures highlight conformational switches required for Mnk activation (Figure 6). The structure of Mnk1-KR represents the fully autoinhibited state (Figure 6,I). Before ATP can bind, the activation segment has to be detached from the N-terminal lobe (unlocking). The structure of Mnk2-KR delineates conformational changes accompanying this relocation (II): the interlobal cleft opens up, Phe230/Phe265 (Mnk1/Mnk2) is removed from the DFG/D-in pocket and the Lys–Glu ion pair can be formed. In the absence of ATP, the DFD motif may retain the DFG/D-out conformation owing to the favorable interactions involving the Mnk-specific DFD-Asp and torsional restraints. After unlocking, ATP can bind and force the DFD-motif into the DFG/D-in conformation, as inferred from the cocrystal structure of Mnk2-KR^{D228G} with staurosporine (III). To adopt the active state, a further inward switch of the P + 1 loop and helix αEF is required (Nolen *et al*, 2004). In the Mnk2-KR crystals, the interactions between neighboring molecules involve the P + 1 loop and helix αEF and closely resemble the intramolecular packing of these elements in active-state kinases (Jauch *et al*, 2005), thus allowing modeling of the active state (IV). We further assume a reclosure of the interlobal cleft in the active state, which would bring residues from the N-terminal lobe such as the GR-loop and the Lys–Glu pair to their catalytic positions.

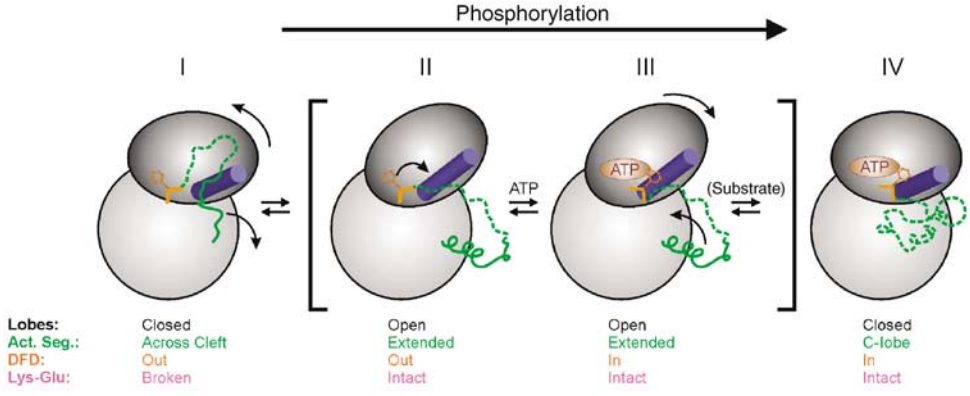

Figure 6 Model for the mechanistic dynamics during Mnk activation. Schematics depicting structural changes required for Mnk activation. The two lobes of the kinase domain are shown as ellipses. Functional elements are color-coded as before. I—autoinhibited state (based on the Mnk1-KR structure); II—structural consequences upon detaching the activation segment from the N-terminal lobe (based on the Mnk2-KR structure); III—DFG/D-in-to-out switch upon ATP binding (based on the Mnk2-KR^{D228G}–staurosporine structure); IV—active state (model). Regions of the activation segment that were disordered in the crystal structures are shown as dashed lines and in arbitrary conformations. The activation segment of the active state (IV) has been modeled based on the crystal packing interaction involving the activation segment in the Mnk2-KR structure (Jauch *et al*, 2005). II and III have been put in brackets because they may not be stable intermediates *in vivo* or the sequence of structural changes may be different.

The ensemble of Mnk structures suggests that the conformational switches required for Mnk activation (Figure 6) can be fired in a stepwise fashion *in vitro*. However, *in vivo* the conformational changes do not have to occur in precisely the order depicted and do not necessarily involve stable intermediates. For example, after phosphorylation, several steps could occur concomitantly or positioning of the P + 1 loop and helix αEF at the C-terminal lobe and peptide substrate binding could take place before ATP binding.

Finally, our observations have direct implications for the design of Mnk-specific inhibitors. To date, the DFG/D-out conformation has been observed in only about 10% of the more than 50 PKs for which structural data are available (Mol *et al*, 2004b; Vieth *et al*, 2005). In rare cases, the DFG/D-out conformation is adopted in the absence of ligands, as first seen in IRK (Hubbard *et al*, 1994). More often it is induced or stabilized by the binding of selective inhibitors such as in the structures of p38 with Birb796 (Pargellis *et al*, 2002), c-Abl with Gleevec (Nagar *et al*, 2002) and VEGFR-2 with AAL-993 (Manley *et al*, 2004). Inhibitors inducing the DFG/D-out conformation by targeting the DFG/D-in pocket are expected to bind with higher selectivity compared to classical compounds, which resemble the binding mode of ATP (Mol *et al*, 2004b). In Mnks, the Phe from the specific insertion I2 points out a selective binding surface (the DFG/D-in pocket) that could be exploited for the design of specific inhibitors. The selectivity of this site is further enhanced by the Mnk-specific DFD-Asp in the vicinity.

Materials and methods

Cloning and protein preparation

A cDNA fragment encoding amino acids 37–341 of human Mnk1 was amplified using the forward/reverse primer pair 5′-CGGGATCC ACTGACTCCTTGCCAGGAAAG/5′ACGCGTCGACCTATCCCTTTTCT GGAGCTTGCC (restriction sites underlined) and was cloned into the *Bam*HI and SalI sites of vector pGEX-4T1 (Amersham Biosciences). This construct allowed expression of Mnk1-KR in *E. coli* as a fusion protein with a N-terminal, thrombin-cleavable glutathione *S*-transferase (GST) tag. Mutations to produce Mnk1-KR variants, in which either Phe230 was converted to Ala (Mnk1-KR^{F230A}) or in which residues 228–232 were deleted (Mnk1-KR$^{\Delta I2}$), were introduced by the QuikChange strategy (Stratagene). The expression and purification of Mnk1-KR and Mnk1-KR variants were identical to the methods described for Mnk2-KR and Mnk2-KR^{D228G} (Jauch *et al*, 2005).

Crystallization and data collection

Wt Mnk1-KR was crystallized at 20°C by vapor diffusion with a reservoir solution containing 20% (w/v) PEG3350, 0.2 M ammonium sulfate and 0.1 M Na-citrate, pH 5.6. Crystals were frozen in a liquid nitrogen stream after transfer into reservoir solution supplemented with 20% glycerol. Crystals of Mnk2-KR^{D228G} were grown as described previously (Jauch *et al*, 2005) and were soaked for 24 h in a 300 μM solution of staurosporine (Sigma-Aldrich) in mother liquor supplemented with 5% (v/v) dimethylsulfoxide. Soaked crystals were cryo-protected and frozen as the underivatized variants (Jauch *et al*, 2005). Diffraction data for Mnk1-KR and Mnk2-KR^{D228G}–staurosporine (Table I) were collected at the PXI and PXII beam lines of the Swiss Light Source (Villigen, Switzerland) at 100 K on a MarResearch CCD detector and processed with the HKL package (Otwinowski and Minor, 1997) (Table I).

Structure solution and refinement

The Mnk1-KR structure was solved by molecular replacement (Collaborative Computational Project, 1994) using a truncated version of Mnk2-KR (Jauch *et al*, 2005) as the search model. The initial electron density was modified by solvent flattening and noncrystallographic symmetry (NCS) averaging (Collaborative Computational Project, 1994). Model building was conducted manually with COOT (Emsley and Cowtan, 2004). Refinement was performed with CNS (Brunger *et al*, 1998) and Refmac5 (Collaborative Computational Project, 1994). Initially, refinement made use of NCS restraints that were omitted in later cycles. All data between 30.0 and 2.5 Å resolution were employed in the refinement, setting aside 5% of the reflections to monitor the free *R*-factor (Table I). The R_{free} set was maintained upon switching refinement programs. Monitoring data completeness in 0.1 Å resolution shells showed that the effective resolution of the structure was 2.8 Å. However, the density was further improved by including all data up to 2.5 Å resolution in the refinement process.

The Mnk2-KR^{D228G}–staurosporine cocrystal structure was solved by molecular replacement using the Mnk2-KR coordinates. Model building and refinement were conducted as for Mnk1-KR using all data between 30.0 and 2.7 Å resolution and with 5% of the reflections monitoring the free *R*-factor (Table I). Staurosporine was added during later refinement cycles to a patch of Fo−Fc difference electron density that was already clearly defined at the onset of refinement.

NMR nucleotide binding assays

One-dimensional ^{1}H spectra and STD-NMR spectra were recorded at 30°C on a Bruker Avance-600 spectrometer equipped with a 5 mm cryogenic probe head. NMR samples contained the respective enzyme (nonphosphorylated Mnk1-KR, nonphosphorylated GST-Mnk1-KR, nonphosphorylated GST-Mnk1-KR^{F230A}, nonphosphorylated GST-Mnk1-KR$^{\Delta I2}$, phosphorylated GST-Mnk1-KR, nonphosphorylated Mnk2-KR, nonphosphorylated Mnk2-KR^{D228G} or phosphorylated Mnk2-KR) without or with AMPPNP (Sigma-Aldrich, 95% purity). All NMR samples were prepared in 10 mM Tris-d, 2 mM $MgCl_2$, 100 mM NaCl, 1 mM dithiothreitol in 99.8% D_2O at pH 7.5 (uncorrected for isotope effects) and were adjusted to a protein concentration of 20 μM based on the absorption at 280 nm. The concentration of AMPPNP was increased stepwise from 0.6 mM to 1.0 mM, corresponding to protein:AMPPNP ratios of 1:30, 1:40, 1:50. At higher AMPPNP concentrations, partial aggregation of AMPPNP was observed. At the end of the AMPPNP titration staurosporine was added.

STD-NMR spectra were acquired using a series of 60 equally spaced 50-ms Gaussian-shaped pulses for selective saturation with a total duration of 3 s. The radiofrequency field strength for the selective saturation pulses was 22 Hz. The frequencies of the protein on-resonance and off-resonance saturation were set to 1.7 and −17 p.p.m., respectively. Similar results were obtained with an on-resonance saturation frequency of 0.352 p.p.m. To suppress residual protein signal, a $T_{1\rho}$-filter comprising a spin lock pulse of 50 ms was applied. Using a recycle delay of 5 s and eight dummy scans, 512 total scans were recorded for each experiment. NMR spectra were multiplied by an exponential window function with a 2.0 Hz line broadening factor before Fourier transformation. Bruker Topspin v. 1.3 was used for processing and analysis of NMR spectra. Fractional STD effects were evaluated as I_{STD}/I_{ref}, in which I_{STD} is the difference of the intensities of a signal in the on- and off-resonance spectra, and I_{ref} is the intensity of the corresponding signal in the off-resonance spectrum (Mayer and Meyer, 2001).

Control experiments that resulted in no observable STD-NMR signal included measuring (i) a sample of only AMPPNP at a concentration of 1.5 mM and (ii) a sample of GST (not expected to bind AMPPNP) and AMPPNP at a ratio of 1:50.

Data deposition

Coordinates and structure factors have been submitted to the RSCB Protein Databank (http://www.rcsb.org/pdb/) with accession codes 2HW6 (Mnk1-KR) and 2HW7 (Mnk2-KR^{D228G}–staurosporine) and will be released upon publication.

Acknowledgements

We thank Reinhard Lührmann for the use of his infrastructure, Monique Erling for excellent technical support and Ehmke Pohl and Clemens Schulze-Briese (beam lines PXI and PXII, Swiss Light Source, Villigen, Switzerland) for help with diffraction data collection. Work was in part supported by the Max-Planck-Gesellschaft (HJ and MCW), an Emmy Noether Fellowship (ZW 71/1–5) from the Deutsche Forschungsgemeinschaft (MZ), a fellowship (GK 782) from the Deutsche Forschungsgemeinschaft (MKC) and a fellowship from the Boehringer Ingelheim Fonds (CN). We declare that we have no competing financial interests.

References

Adams JA (2001) Kinetic and catalytic mechanisms of protein kinases. *Chem Rev* **101:** 2271–2290

Brunger AT, Adams PD, Clore GM, DeLano WL, Gros P, Grosse-Kunstleve RW, Jiang JS, Kuszewski J, Nilges M, Pannu NS, Read RJ, Rice LM, Simonson T, Warren GL (1998) Crystallography & NMR system: A new software suite for macromolecular structure determination. *Acta Crystallogr D* **54:** 905–921

Buxade M, Parra JL, Rousseau S, Shpiro N, Marquez R, Morrice N, Bain J, Espel E, Proud CG (2005) The Mnks are novel components in the control of TNFalpha biosynthesis and phosphorylate and regulate hnRNP A1. *Immunity* **23:** 177–189

Canagarajah BJ, Khokhlatchev A, Cobb MH, Goldsmith EJ (1997) Activation mechanism of the MAP kinase ERK2 by dual phosphorylation. *Cell* **90:** 859–869

Collaborative Computational Project N (1994) The CCP4 Suite: programs for protein crystallography. *Acta Crystallogr D* **50:** 760–763

Dar AC, Dever TE, Sicheri F (2005) Higher-order substrate recognition of eIF2alpha by the RNA-dependent protein kinase PKR. *Cell* **122:** 887–900

Emsley P, Cowtan K (2004) Coot: model-building tools for molecular graphics. *Acta Crystallogr D* **60:** 2126–2132

Flocco MM, Mowbray SL (1995) Strange bedfellows: interactions between acidic side-chains in proteins. *J Mol Biol* **254:** 96–105

Fukunaga R, Hunter T (1997) MNK1, a new MAP kinase-activated protein kinase, isolated by a novel expression screening method for identifying protein kinase substrates. *EMBO J* **16:** 1921–1933

Goldberg J, Nairn AC, Kuriyan J (1996) Structural basis for the autoinhibition of calcium/calmodulin-dependent protein kinase I. *Cell* **84:** 875–887

Griffith J, Black J, Faerman C, Swenson L, Wynn M, Lu F, Lippke J, Saxena K (2004) The structural basis for autoinhibition of FLT3 by the juxtamembrane domain. *Mol Cell* **13:** 169–178

Hanks SK (2003) Genomic analysis of the eukaryotic protein kinase superfamily: a perspective. *Genome Biol* **4:** 111

Hanks SK, Quinn AM, Hunter T (1988) The protein kinase family: conserved features and deduced phylogeny of the catalytic domains. *Science* **241:** 42–52

Hubbard SR, Wei L, Ellis L, Hendrickson WA (1994) Crystal structure of the tyrosine kinase domain of the human insulin receptor. *Nature* **372:** 746–754

Huse M, Kuriyan J (2002) The conformational plasticity of protein kinases. *Cell* **109:** 275–282

Jauch R, Jäkel S, Netter C, Schreiter K, Aicher B, Jäckle H, Wahl M (2005) Crystal structures of the Mnk2 kinase domain reveal an inhibitory conformation and a Zinc-binding site. *Structure* **13:** 1559–1568

Jeffrey PD, Russo AA, Polyak K, Gibbs E, Hurwitz J, Massague J, Pavletich NP (1995) Mechanism of CDK activation revealed by the structure of a cyclinA–CDK2 complex. *Nature* **376:** 313–320

Knighton DR, Zheng JH, Ten Eyck LF, Ashford VA, Xuong NH, Taylor SS, Sowadski JM (1991) Crystal structure of the catalytic subunit of cyclic adenosine monophosphate-dependent protein kinase. *Science* **253:** 407–414

Kobe B, Heierhorst J, Feil SC, Parker MW, Benian GM, Weiss KR, Kemp BE (1996) Giant protein kinases: domain interactions and structural basis of autoregulation. *EMBO J* **15:** 6810–6821

Krupa A, Preethi G, Srinivasan N (2004) Structural modes of stabilization of permissive phosphorylation sites in protein kinases: distinct strategies in Ser/Thr and Tyr kinases. *J Mol Biol* **339:** 1025–1039

Lawrie AM, Noble ME, Tunnah P, Brown NR, Johnson LN, Endicott JA (1997) Protein kinase inhibition by staurosporine revealed in details of the molecular interaction with CDK2. *Nat Struct Biol* **4:** 796–801

Manley PW, Bold G, Bruggen J, Fendrich G, Furet P, Mestan J, Schnell C, Stolz B, Meyer T, Meyhack B, Stark W, Strauss A, Wood J (2004) Advances in the structural biology, design and clinical development of VEGF-R kinase inhibitors for the treatment of angiogenesis. *Biochim Biophys Acta* **1697:** 17–27

Manning G, Whyte DB, Martinez R, Hunter T, Sudarsanam S (2002) The protein kinase complement of the human genome. *Science* **298:** 1912–1934

Mayer M, Meyer B (2001) Group epitope mapping by saturation transfer difference NMR to identify segments of a ligand in direct contact with a protein receptor. *J Am Chem Soc* **123:** 6108–6117

McCoy MA, Senior MM, Wyss DF (2005) Screening of protein kinases by ATP-STD NMR spectroscopy. *J Am Chem Soc* **127:** 7978–7979

Mol CD, Dougan DR, Schneider TR, Skene RJ, Kraus ML, Scheibe DN, Snell GP, Zou H, Sang BC, Wilson KP (2004a) Structural basis for the autoinhibition and STI-571 inhibition of c-Kit tyrosine kinase. *J Biol Chem* **279:** 31655–31663

Mol CD, Fabbro D, Hosfield DJ (2004b) Structural insights into the conformational selectivity of STI-571 and related kinase inhibitors. *Curr Opin Drug Discov Dev* **7:** 639–648

Nagar B, Bornmann WG, Pellicena P, Schindler T, Veach DR, Miller WT, Clarkson B, Kuriyan J (2002) Crystal structures of the kinase domain of c-Abl in complex with the small molecule inhibitors PD173955 and imatinib (STI-571). *Cancer Res* **62:** 4236–4243

Nikolcheva T, Pyronnet S, Chou SY, Sonenberg N, Song A, Clayberger C, Krensky AM (2002) A translational rheostat for RFLAT-1 regulates RANTES expression in T lymphocytes. *J Clin Invest* **110:** 119–126

Nolen B, Taylor S, Ghosh G (2004) Regulation of protein kinases; controlling activity through activation segment conformation. *Mol Cell* **15:** 661–675

Notredame C, Higgins DG, Heringa J (2000) T-Coffee: a novel method for fast and accurate multiple sequence alignment. *J Mol Biol* **302:** 205–217

O'Loghlen A, Gonzalez VM, Pineiro D, Perez-Morgado MI, Salinas M, Martin ME (2004a) Identification and molecular characterization of Mnk1b, a splice variant of human MAP kinase-interacting kinase Mnk1. *Exp Cell Res* **299:** 343–355

O'Loghlen A, Gonzalez VM, Salinas M, Martin ME (2004b) Suppression of human Mnk1 by small interfering RNA increases the eukaryotic initiation factor 4F activity in HEK293 T cells. *FEBS Lett* **578:** 31–35

Otwinowski Z, Minor W (1997) Processing of X-ray diffraction data collected in oscillation mode. *Methods Enzymol* **276:** 307–326

Pargellis C, Tong L, Churchill L, Cirillo PF, Gilmore T, Graham AG, Grob PM, Hickey ER, Moss N, Pav S, Regan J (2002) Inhibition of p38 MAP kinase by utilizing a novel allosteric binding site. *Nat Struct Biol* **9:** 268–272

Parra JL, Buxade M, Proud CG (2005) Features of the catalytic domains and C termini of the MAPK signal-integrating kinases Mnk1 and Mnk2 determine their differing activities and regulatory properties. *J Biol Chem* **280:** 37623–37633

Prade L, Engh RA, Girod A, Kinzel V, Huber R, Bossemeyer D (1997) Staurosporine-induced conformational changes of cAMP-dependent protein kinase catalytic subunit explain inhibitory potential. *Structure* **5:** 1627–1637

Reiling JH, Doepfner KT, Hafen E, Stocker H (2005) Diet-dependent effects of the *Drosophila* Mnk1/Mnk2 homolog Lk6 on growth via eIF4E. *Curr Biol* **15:** 24–30

Russo AA, Jeffrey PD, Pavletich NP (1996) Structural basis of cyclin-dependent kinase activation by phosphorylation. *Nat Struct Biol* **3:** 696–700

Scheper GC, Morrice NA, Kleijn M, Proud CG (2001) The mitogen-activated protein kinase signal-integrating kinase Mnk2 is a eukaryotic initiation factor 4E kinase with high levels of basal activity in mammalian cells. *Mol Cell Biol* **21:** 743–754

Scheper GC, Parra JL, Wilson M, Van Kollenburg B, Vertegaal AC, Han ZG, Proud CG (2003) The N and C termini of the splice variants of the human mitogen-activated protein kinase-interacting kinase Mnk2 determine activity and localization. *Mol Cell Biol* **23:** 5692–5705

Slentz-Kesler K, Moore JT, Lombard M, Zhang J, Hollingsworth R, Weiner MP (2000) Identification of the human Mnk2 gene (MKNK2) through protein interaction with estrogen receptor beta. *Genomics* **69:** 63–71

Tamaoki T, Nomoto H, Takahashi I, Kato Y, Morimoto M, Tomita F (1986) Staurosporine, a potent inhibitor of phospholipid/Ca + + dependent protein kinase. *Biochem Biophys Res Commun* **135:** 397–402

Taylor SS, Radzio-Andzelm E (1994) Three protein kinase structures define a common motif. *Structure* **2:** 345–355

Tereshko V, Teplova M, Brunzelle J, Watterson DM, Egli M (2001) Crystal structures of the catalytic domain of human protein

kinase associated with apoptosis and tumor suppression. *Nat Struct Biol* **8:** 899–907

Ueda T, Watanabe-Fukunaga R, Fukuyama H, Nagata S, Fukunaga R (2004) Mnk2 and Mnk1 are essential for constitutive and inducible phosphorylation of eukaryotic initiation factor 4E but not for cell growth or development. *Mol Cell Biol* **24:** 6539–6549

Vieth M, Sutherland JJ, Robertson DH, Campbell RM (2005) Kinomics: characterizing the therapeutically validated kinase space. *Drug Discov Today* **10:** 839–846

Walsh D, Mohr I (2004) Phosphorylation of eIF4E by Mnk-1 enhances HSV-1 translation and replication in quiescent cells. *Genes Dev* **18:** 660–672

Waskiewicz AJ, Flynn A, Proud CG, Cooper JA (1997) Mitogen-activated protein kinases activate the serine/threonine kinases Mnk1 and Mnk2. *EMBO J* **16:** 1909–1920

Waskiewicz AJ, Johnson JC, Penn B, Mahalingam M, Kimball SR, Cooper JA (1999) Phosphorylation of the cap-binding protein eukaryotic translation initiation factor 4E by protein kinase Mnk1 *in vivo*. *Mol Cell Biol* **19:** 1871–1880

Werten S, Mitschler A, Romier C, Gangloff YG, Thuault S, Davidson I, Moras D (2002) Crystal structure of a subcomplex of human transcription factor TFIID formed by TATA binding protein-associated factors hTAF4 (hTAF(II)135) and hTAF12 (hTAF(II)20). *J Biol Chem* **277:** 45502–45509

